ELSEVIER

Journal of Volcanology and Geothermal Research 86 (1998) 107–115

Journal of volcanology and geothermal research

Orientation distribution of microlites in obsidian

Michael Manga *

Department of Geological Sciences, University of Oregon, Eugene, OR 97403, USA

Revised 16 June 1998

Abstract

The shape and three-dimensional orientation distribution of microlites are measured in obsidian from Little Glass Mountain, CA. Measurements are made from thin sections using an image series of high magnification digital micrographs taken serially through different focal depths. These measurements agree well with the theoretically predicted and experimentally measured distribution of long slender rods in a Newtonian fluid undergoing simple shear flow. In this type of flow, rods in a dilute suspension rotate periodically, spending most of the time aligned with the flow. Measurements of the detailed orientation distribution integrated with theoretical models provide a tool for inferring flow dynamics and the timing of magmatic processes.

Keywords: microlites; obsidian; flow dynamics; magmatic processes

1. Introduction

The nature of magmatic processes, such as solidification, degassing and flow behavior, are often inferred from the textures and structures preserved in volcanic rocks. Measured vesicle-size distributions, for example, can be used to infer eruption parameters, such as nucleation depth and ascent velocity (Toramaru, 1989), and crystal-size distributions can be used to infer solidification rates (Cashman, 1993). Preferred orientations and imbricated crystals can also be used to infer strains (e.g., Shelley, 1985; Smith et al., 1994; Ventura et al., 1996). Here, I examine the three-dimensional orientation distribution of rod-shaped albite microlites in obsidian, and consider the relationship between microlite orientation and properties of the flow.

The goal here is to show how measured orientation distributions can be interpreted within a theoretical framework. I begin by reviewing the dynamics of long slender particles in shear flows, including research results from the last few years. Next, a new method is presented for quantifying the three-dimensional orientation of microlites; the technique is then applied to an obsidian sample from Little Glass Mountain, CA. Agreement between measured and theoretical distributions suggests that the technique may be useful in determining the emplacement history and dynamics of obsidian flows, when applied to a representative suite of oriented samples.

* Tel.: +1-541-346-5574; Fax: +1-541-346-4692; E-mail: manga@newberry.uoregon.edu

0377-0273/98/$19.00
PII: S0377-0273(98)00084-5

2. Orientation of microlites: theoretical considerations

Consider a rod-shaped particle immersed in a flow, $\mathbf{u}^{\text{ext}}$, in which inertial forces can be neglected. Specifically, the Reynolds number of the rod, GL^2/ν is $\ll 1$, where G is the magnitude of the local strain rate, L is the rod's length, and ν is the kinematic viscosity of the liquid.

I consider two end-member flows, a pure shear flow:

$$\mathbf{u}^{\text{ext}} = (Gx, -Gy, 0), \tag{1}$$

and a simple shear flow:

$$\mathbf{u}^{\text{ext}} = (Gy, 0, 0). \tag{2}$$

Here, $\mathbf{u}^{\text{ext}} = (u_x^{\text{ext}}, u_y^{\text{ext}}, u_z^{\text{ext}})$, and x, y and z indicate distances in the coordinate system shown in Fig. 1a. For the pure shear flow, the x direction is the direction of extension; for the simple shear flow, the x direction is the flow direction and vorticity is in the z direction. Two angles are defined in order to characterize the orientation of the rod: ϕ, measured from the y direction, and θ, measured from the z direction.

Jeffery (1922) first solved the equations of motion for an axisymmetric ellipsoidal particle in a low-Reynolds-number simple shear flow and found that such a particle will rotate with period:

$$T = 2\pi(R_1 + 1/R_1)/G, \tag{3}$$

where R_1 is the aspect ratio of the ellipsoid. Bretherton (1962) showed that the equations developed by Jeffery (1922) apply to any axisymmetric object and that the dynamics of rod-shaped particles is equivalent to the dynamics of ellipsoids with aspect ratio $R_1 \approx 1.35R_r$, where R_r denotes the aspect ratio of the rod. Nonaxisymmetric particles may undergo either chaotic, periodic or quasi-periodic rotations (Yarin et al., 1997).

The differential equations governing the motion of particles in a simple shear flow are (e.g., Jeffery, 1922):

$$\frac{\mathrm{d}\phi}{\mathrm{d}t} = \frac{G}{R_1^2 + 1}\left(R_1^2\cos^2\phi + \sin^2\phi\right) \tag{4}$$

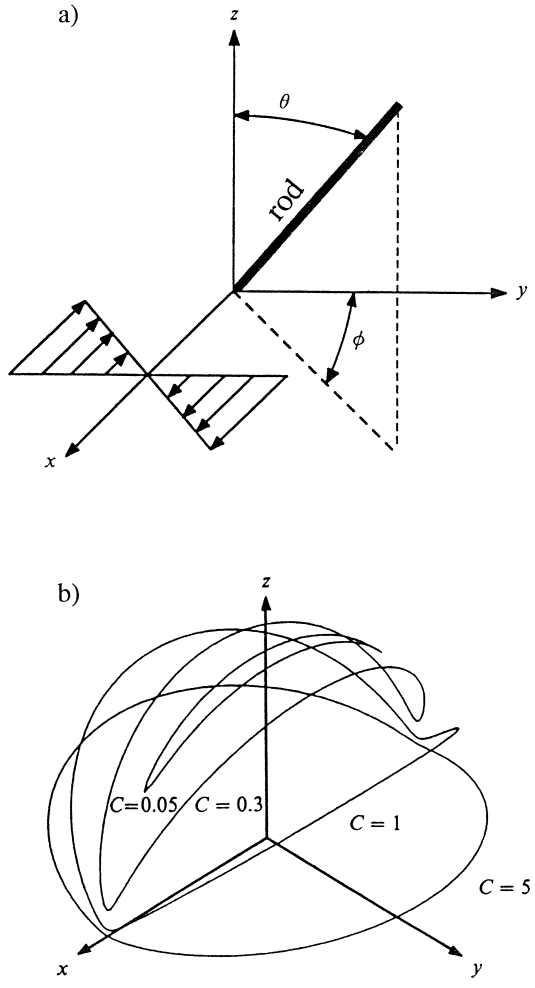

Fig. 1. (a) Definition of coordinate system, orientation angles θ and ϕ, and the direction of the simple shear flow considered here, Eq. (2). (b) Illustration of Jeffery orbits for different values of the orbit constant C.

and

$$\frac{\mathrm{d}\theta}{\mathrm{d}t} = G\frac{R_1^2 - 1}{R_1^2 + 1}\sin\theta\cos\theta\sin\phi\cos\phi, \tag{5}$$

where t is time. Each of these closed trajectories (sometimes called Jeffery orbits) can be conveniently characterized by an 'orbit constant' (Fig. 1b):

$$C = \frac{\tan\theta\left(R_1^2\cos^2\phi + \sin^2\phi\right)^{\frac{1}{2}}}{R_1}. \tag{6}$$

The analogous expressions to Eqs. (4) and (5) for a pure shear flow are (e.g., Gay, 1966):

$$\frac{\mathrm{d}\phi}{\mathrm{d}t} = G\frac{R_l^2 - 1}{R_l^2 + 1}\sin 2\phi \tag{7}$$

and

$$\frac{\mathrm{d}\theta}{\mathrm{d}t} = -\frac{1}{2}\cot 2\phi \sin 2\theta \frac{\mathrm{d}\phi}{\mathrm{d}t}. \tag{8}$$

Whereas particles in a simple shear flow rotate continuously, particles in a pure shear flow become, and remain, aligned in the direction of extension.

In order to highlight the difference in orientation distributions between pure and simple shear flows, calculated distributions are shown in Fig. 2 for ellipsoids with aspect ratio $R_l = 10$. I assume the particles are initially randomly oriented and do not interact hydrodynamically. I obtain these theoretical distributions by integrating the equations of motion Eqs. (4), (5), (7) and (8) for one million random initial orientations. The orientation distribution is characterized by the standard deviations σ_θ and σ_ϕ of the angles θ and ϕ, respectively. In the pure shear flow, all particles become aligned with the direction of extension and both σ_θ and σ_ϕ approach zero. In the simple shear flow, however, σ_θ and σ_ϕ approach finite constants. The actual distributions of ϕ and θ for the simple shear flow are shown later.

The equations presented above apply only if the suspension is sufficiently dilute (volume fractions $c \ll 1$) that hydrodynamic interactions among the particles can be neglected. Suspensions of rods are called 'dilute' if $nL^3 \ll 1$, where n is the number density, i.e., number of microlites per unit volume (e.g., Batchelor, 1971). In the so-called 'semidilute' limit, nL^3 is no longer $\ll 1$, but $nL^2 d < 1$, where d is the rod's diameter (e.g., Fredrickson and Shaqfeh, 1989). In the semidilute limit, particles are still separated by many particle diameters, but not by many particle lengths. The effects of interactions between particles on their orientation is discussed in more detail below.

Finally, I note that the two flows considered here are only end members, and in general, flows will involve a combination of both pure and simple shear. Due to the linearity of the equations of motion governing flow at Reynolds numbers $\ll 1$, Eqs. (4), (5), (7) and (8) can be added linearly to describe the evolution of particle orientation.

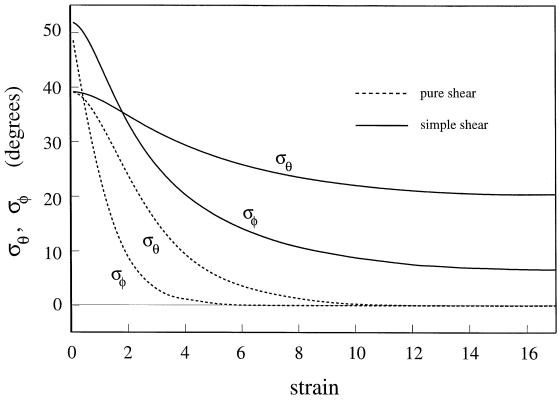

Fig. 2. Standard deviation σ_θ and σ_ϕ of the angles θ and ϕ as a function of strain for a pure shear (dashed curves) and simple shear (solid curves).

3. Orientation distribution: measurements

Two thin sections were prepared from a single sample of obsidian from the Little Glass Mountain, CA, obsidian flow. The sample was collected from the front of the flow. The sample is visually 'flow' banded, and contains alternating 'dark' and 'light' bands ranging in thickness from less than 1 mm to about 5 mm. The color differences result from variations in microlite crystallinity. The thin sections were cut both parallel to the flow direction inferred from the orientation of stretched vesicles and perpendicular to the layering represented by the flow bands. In this particular sample, microlites are oriented parallel to the flow bands (x direction); however, this is not always the case (Fink, 1983).

Because the particle orbits determined by Eqs. (4), (5), (7) and (8) are fully three-dimensional, the three-dimensional orientation of microlites must also be measured. In addition, a justified interpretation of preferred orientations requires ''simultaneous measurements of both grain shapes and grain orientations'' (Willis, 1977) due to the dependence of particle dynamics on their aspect ratio.

The measurement technique involves making a set of high-magnification (500×) digital photomicro-

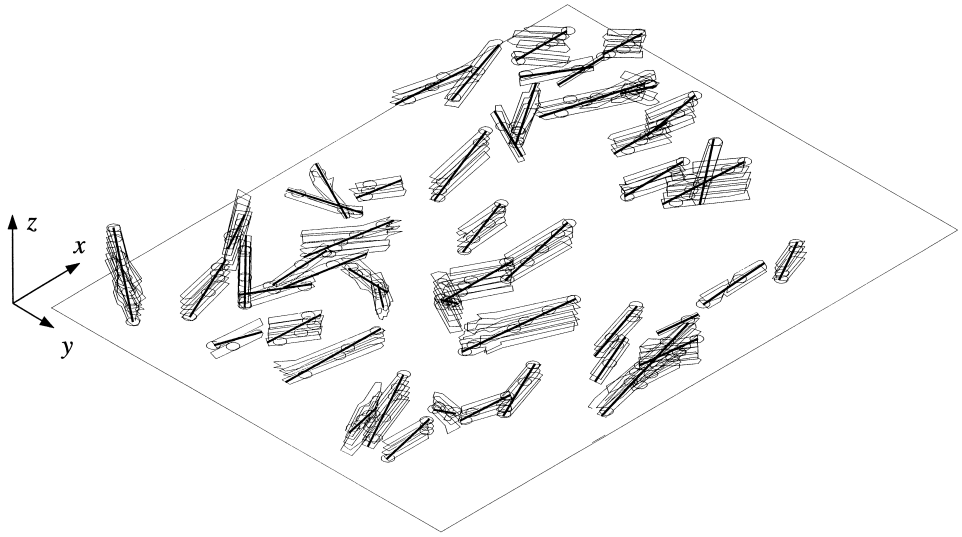

Fig. 3. Example of a set of stacked set of digitized images taken from various focal depths within a thin section. Sample is from the Big Obsidian Flow at Newberry, Oregon. The bold lines represent the orientation of the microlites, the thin curves are traces of the microlites in each image. The disks show the position of the focussed part of each microlite in each image.

graphs at 2-μm depth intervals from the bottom focal plane to the upper focal plane of the thin section. For a given image, the outline of each microlite is digitized in a computer-assisted drafting (CAD) program. In each image a point marker is placed at the focal point of each microlite, that is, the position at which each microlite is most in focus. The images are stacked as a set of layers in the CAD program and the upper and lower focal points of each microlite are connected. The CAD program can then be used to calculate the orientation, width, and length of each microlite. Fig. 3 shows a stacked set of digitized images in order to illustrate the measurement procedure. The sample in Fig. 3 is from the Big Obsidian Flow at Newberry volcano, OR, and is used for illustrative purposes because of its relatively low density of microlites.

Table 1 summarizes measured geometrical properties of the microlites in the Little Glass Mountain thin sections. I estimate the uncertainties in measurements of ϕ and θ to be about 1° and 5°, respectively. The much larger uncertainty of θ is due to the limited depth resolution that can be obtained with 2-μm focusing intervals.

The measurement technique employed here has several advantages compared to previous techniques for measuring three-dimensional orientations (e.g., Shelley, 1985; Wada, 1992): all possible orientations can be measured, orientation and shape are simultaneously determined for each crystal, and measurements can be made for all the crystals within the chosen volume. In Fig. 4, I show examples of digital photomicrographs from both thin sections along with the measured orientation distributions projected onto three different planes. In the x–y plane (see Fig. 1a for a definition of axes), the microlites are well-aligned and are parallel to the macroscopic flow banding. Orientations in the other two planes are more scattered. Finally, the measurement procedure

Table 1
Microlite properties of the two obsidian thin sections

Property	Section A	Section B
Number of microlites	166	475
Volume fraction, c	0.0058	0.014
Number density, n (m^{-3})	1.63×10^{14}	6.34×10^{14}
Mean length, L (μm)	17.3	18.5
Mean diameter, d (μm)	1.22	1.47
nL^3	0.83	4.0
nL^2d	0.059	0.30

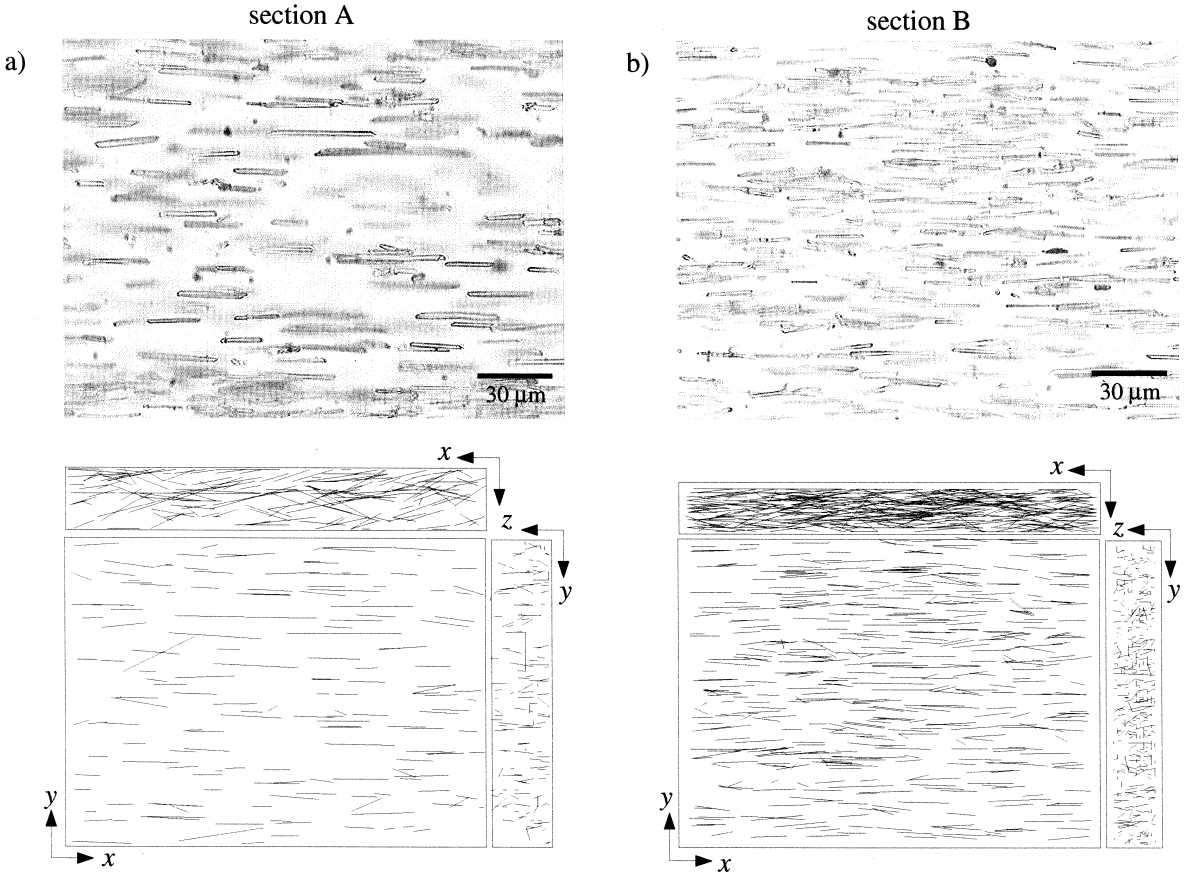

Fig. 4. Examples of photomicrographs (top) and projections (bottom) of the three-dimensional measured microlite orientations onto three orthogonal planes. Sample is from Little Glass Mountain, CA. (a) and (b) correspond to thin sections from light- and dark-colored bands, respectively.

described here also produces the three-dimensional crystal size distribution (CSD). It is beyond the scope of this paper to interpret the CSDs.

4. Orientation distribution: measurements compared with theory

In both pure and simple shear flows, microlites tend to become oriented subparallel to the flow. In a simple shear flow, a steady-state distribution of orientations is obtained (Fig. 2). By contrast, in pure shear flows, microlites will eventually become nearly perfectly aligned; in fact, the effect of particle–particle interactions will be to promote alignment (Gay, 1966). Below, I argue that the orientation distribution of Little Glass Mountain microlites is dominated by simple shear flow, and then compare the detailed theoretical and measured distributions.

The interaction between microlites and a phenocryst is shown in Fig. 5. On the right, I show half of a rounded phenocryst from the same Little Glass Mountain obsidian sample; on the left, I show calculated streamlines for simple shear flow around a rigid sphere. Surrounding such a sphere there is a region of fluid that remains near, and rotates with, the sphere (the stippled region); this region would not exist in a pure shear flow (see inset of Fig. 5). The calculated streamlines in Fig. 5 and the inset correspond to flow around a sphere in an external flow described by Eqs. (2) and (1), respectively (see Leal (1992) for the detailed velocity solutions). Comparing microlite orientations and streamlines for

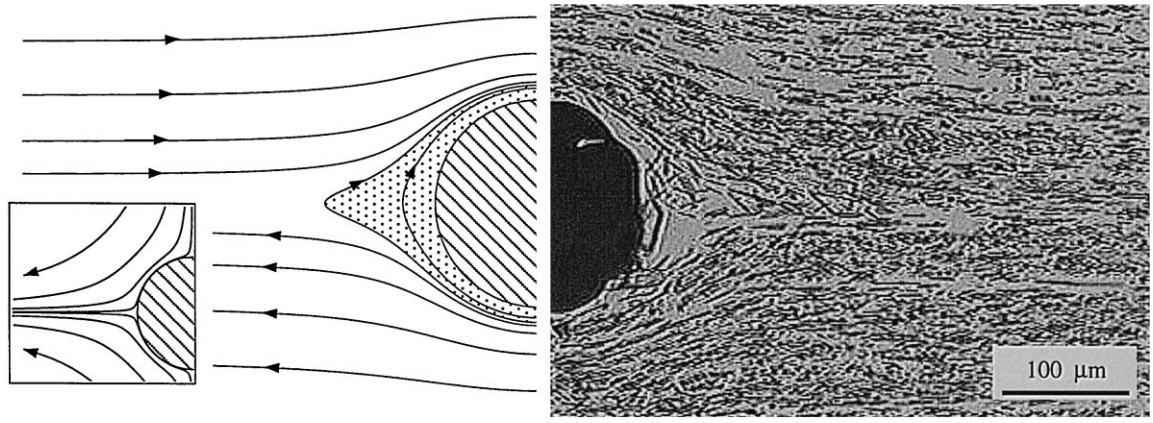

Fig. 5. Left: Calculated streamlines for simple shear flow around a freely rotating solid sphere. Right: Microlite orientation around a phenocryst. The stippled region on the left contains fluid that remains near, and rotates with, the sphere. Inset: Calculated streamlines for pure shear flow around a solid sphere.

simple shear, I observe similar amounts and patterns of flow distortion by the sphere and phenocryst. There is also a region around the phenocryst (corresponding to the fluid which rotates with the sphere) in which microlite orientations are disturbed. On the basis of the agreement between observed orientations and calculated streamlines for simple shear flow, in the rest of this section, I will assume that flow was predominantly a simple shear flow.

In Fig. 6, I show the measured distribution of ϕ for microlites with aspect ratios in the range $10 < R_r < 20$. Probability distributions are normalized so that the probability distribution integrated over all values is 1. For comparison, I also show the theoretical distribution for different aspect ratios, R_r, assuming the rods are initially randomly oriented and do not interact. I obtain the theoretical distributions for simple shear flow by integrating the equations of motion Eqs. (4) and (5) for 10 million random initial orientations. The theoretical distributions are steady-state results that derive from large strains of greater than about 10 (see Fig. 2). In a pure shear flow, by contrast, the width of the theoretical distribution decreases continuously with increasing strain (Fig. 2) and nearly perfect alignment occurs for strains greater than about 3. The measured ϕ distribution is nearly identical to the theoretical results for simple shear for noninteracting rods; similar agreement is also found in laboratory experiments with both dilute and semidilute fibrous suspensions (Stover et al., 1992).

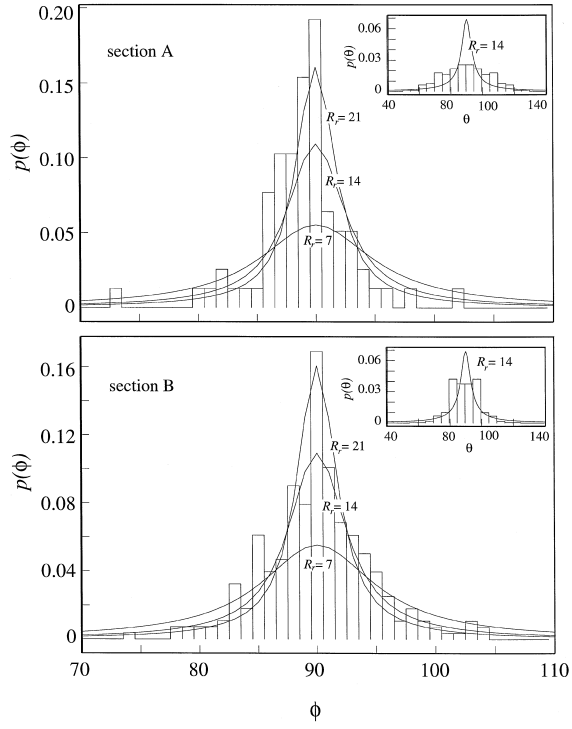

Fig. 6. Measured (histograms) and theoretical (curves) distribution of ϕ. Theoretical results are shown for rod aspect ratios, R_r, of 7, 14 and 21. Measurements are for microlites with aspect ratios between 10 and 20. (a) and (b) correspond to Section A and B in Fig. 2. Inset shows measured (histograms) and theoretical (curves) distribution of θ for the same microlites. Theoretical curves are for aspect ratios of $R_r = 14$.

The slight asymmetry in the ϕ distribution, by about 1°, for sample A (Fig. 6a) may arise because the thin section was not cut exactly perpendicular to the vorticity direction.

The measured θ distribution, along with that expected for noninteracting rods governed by Eqs. (4) and (5), is shown in the inset of Fig. 6. Unlike the ϕ distribution, the measured θ distribution is clearly different from the theoretical distribution. This difference was also observed in experiments with fibers in shear flows, both in the dilute (Anczurowski and Mason, 1979) and semidilute (Stover et al., 1992) regimes; in both cases, the broadening of the θ distribution is attributed to hydrodynamic interactions between the rods. In non-Newtonian, shear-thinning fluids, theoretical results (Leal, 1975) and experimental measurements (Gauthier et al., 1971) have shown that dispersion in the θ distribution is also characteristic of non-Newtonian, shear-thinning fluids, especially for strains greater than about 10 (Ferguson, 1979). However, I show next that the effect of particle–particle interactions in a Newtonian fluid is to produce θ distributions very similar to the measured ones, and it is not necessary to invoke non-Newtonian rheologies to explain the measurements in Fig. 6. Indeed, laboratory experiments have shown that for strain rates less than about 10^{-4} to 10^{-3} s^{-1}, Little Glass Mountain obsidian is Newtonian (Webb and Dingwell, 1990). The mean strain rates during the Little Glass Mountain eruption were probably substantially lower. A strain rate of $> 10^{-3}$ s^{-1} would imply an emplacement time of less than 6 h for the entire flow assuming that the aspect ratio of about 20 for the flow (length of 2 km, thickness of 100 m) implies a total strain of about 20.

Even in dilute suspensions, hydrodynamic interactions between suspended rods result in an orientation dispersion. This dispersion is characterized mathematically by a tensorial diffusion coefficient in the governing differential equation for the probability distribution function describing particle orientation (e.g., Leal and Hinch, 1971). Because the simple shear flow and orientation distribution are anisotropic, there is no reason to expect the orientation diffusion to be isotropic (Stover et al., 1992). Following the notation and terminology of Stover et al. (1992), the diffusivity in the θ and ϕ directions are denoted $D_{\theta\theta}$ and $D_{\phi\phi}$, respectively. Rahnama et al. (1995) find solutions, in terms of the orbit constant C (as in Eq. (6)) and the diffusivity ratio $D_{\theta\theta}/D_{\phi\phi}$, for the orientation distribution which accounts for anisotropic orientation dispersion:

$$p(C_b) = \frac{4C_b\left(\frac{D_{\theta\theta}}{D_{\theta\theta}}\right)}{\left(4\left[\frac{C_b}{1-C_b}\right]^2\frac{D_{\theta\theta}}{D_{\phi\phi}}+1\right)^{3/2}(1-C_b)^3}, \tag{9}$$

where $p(C_b)$ is the probability of a rod having a given value of $C_b = C/(1+C)$. In Fig. 7, I compare the measured distribution of orbit constants with the theoretical model of Rahnama et al. (1995) for $D_{\theta\theta}/D_{\phi\phi} = 4$ and 1.2. The values of $D_{\theta\theta}/D_{\phi\phi}$ used here to generate the curves in Fig. 7 are 'best-fit' values and are not based on theory. The 'best-fit' values of $D_{\theta\theta}/D_{\phi\phi}$ used to explain the experimental measurements of Stover et al. (1992) and Anczurowski and Mason (1979) are similar to the two values used here for their respective concentrations nL^3 (see Fig. 5 in Stover et al., 1992).

Given the resolution of our three-dimensional orientation measurements, there is excellent agreement between measurements and theory for the ϕ orienta-

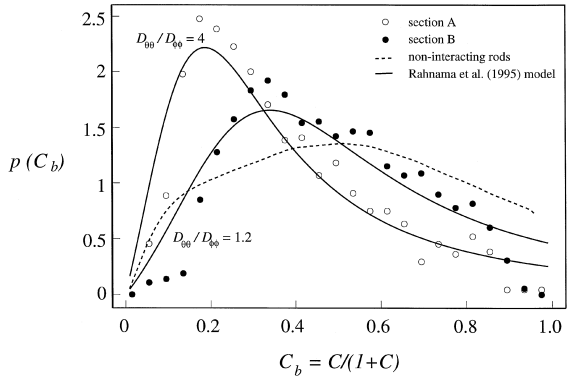

Fig. 7. Distribution of $C_b = C/(1+C)$, where C is the orbit constant defined by Eq. (6) and shown in Fig. 1b. The open and solid points correspond to Sections A and B shown in Fig. 2. The dashed curve is the distribution of C_b for initially randomly oriented microlites moving in Jeffery orbits; the solid curves are model predictions accounting for hydrodynamic orientation distribution (Rahnama et al., 1995).

tion. The overall orientation distribution, characterized by the orbit constant C (Eq. (6)), also agrees well with theoretical predictions if hydrodynamic interactions between microlites in a Newtonian fluid are considered (Fig. 7). Thus, the observed orientation distribution is probably dominated by the reorientation of microlites in a simple shear flow. Implicit in the current analysis is the assumption that microlites formed prior to the flow responsible for the preserved orientation. The history of nucleation and growth during flow will affect the size distribution of microlites (e.g., Marsh, 1988) and possibly their orientation distribution.

5. Concluding remarks

Obsidian domes and flows are common throughout the western USA and represent a major part of the late Holocene volcanic record in the Pacific Northwest. Because ''no geologist has ever witnessed an obsidian in motion'' (Nichols, 1941) constraints on the physical processes and timing of mechanisms responsible for their formation are derived mostly from textural and structural studies (e.g., Christensen and Lipman, 1966; Fink, 1983; Eichelberger et al., 1986; Fink et al., 1992; Smith and Houston, 1994). Microlite orientation is one type of microstructure preserved in obsidian flows that may provide quantitative information about emplacement dynamics.

In comparing measured and calculated orientation distributions I assumed the flow was a simple shear flow (based on Fig. 5). This assumption implies strains greater than about 10 (see Fig. 3). Considering that the sample was collected from the front of the flow, it is not unreasonable to expect that the obsidian experienced strains larger than about 10. Such large strains preserved in microlite orientations would thus imply that at least these microlites formed in the conduit or near the vent, and no (or few) microlites formed after the flow ceased. Indeed, flow bands appear to be ubiquitous (e.g., Manley and Fink, 1987; Swanson et al., 1989) implying that some microlites are present in the conduit. Obsidian flows also exhibit a range of complex flow structures including diapirs and buckle folds (e.g., Fink, 1983; Castro and Cashman, 1996). The total strains associated with folds are generally less than about 1 (J. Castro, personal communication) and the orientation distribution produced by the simple shear associated with flow advance should not be overprinted significantly (see Fig. 2).

In summary, the orientation distribution of microlites presumably reflects the combined history of crystallization and flow. Three-dimensional orientation measurements can be interpreted in terms of the dynamics of microlites in various types of flow, and such an integrated approach can thus potentially provide quantitative insight into magmatic processes that occur during obsidian flow emplacement.

Acknowledgements

C. Ambers developed the procedures for measuring microlite orientation and performed the tedious measurements. K.V. Cashman provided the microscope and image recorder. J. Castro, C. Dorsey and J. Hammer provided comments. The author benefited immensely from comments by M. Mangan. This work was supported by a CAREER grant from NSF. C. Ambers was supported by a grant from the Petroleum Research Fund.

References

Anczurowski, E., Mason, S.G., 1979. The kinetics of flowing dispersion: III. Equilibrium orientations of rods and discs (experimental). J. Colloid Interface Sci. 23, 533–546.

Batchelor, G.K., 1971. The stress generated in a non-dilute suspension of elongated particles by pure straining motion. J. Fluid Mech. 46, 813–829.

Bretherton, F.P., 1962. The motion of rigid particles in a shear flow at low Reynolds number. J. Fluid Mech. 14, 284–304.

Cashman, K.V., 1993. Relationship between plagioclase crystallization and cooling rate in basaltic melts. Contrib. Miner. Petrol. 113, 126–142.

Castro, J.M., Cashman, K.V., 1996. Rheologic behavior of obsidian and coarsely vesicular pumice in Little Glass Mountain and Obsidian Dome, California. EOS 77, 802.

Christensen, M.N., Lipman, P.W., 1966. Emplacement and thermal history of a rhyolite flow near Fortymile Canyon, southern Nevada. Geol. Soc. Am. Bull. 77, 671–684.

Eichelberger, J.C., Carrigan, C.R., Westrich, H.R., Price, R.H., 1986. Non-explosive silicic volcanism. Nature 323, 589–602.

Ferguson, C.C., 1979. Rotations of elongate rigid particles in slow non-Newtonian flows. Tectonophysics 60, 247–262.

Fink, J.H., 1983. Structure and emplacement of a rhyolitic obsidian flow: Little Glass Mountain, Medicine Lake Highland, northern California. Geol. Soc. Am. Bull. 94, 362–380.

Fink, J.H., Anderson, S.W., Manley, C.R., 1992. Textural constraints on effusive silicic volcanism: beyond the permeable foam model. J. Geophys. Res. 97, 77–88.

Fredrickson, G.H., Shaqfeh, E.S.G., 1989. Heat and mass transport in composites of aligned slender fibers. Phys. Fluids A 1, 3–20.

Jeffery, G.B., 1922. The motion of ellipsoidal particles immersed in a viscous fluid. Proc. R. Soc. London A 102, 161–179.

Gauthier, R., Goldsmith, H.L., Mason, S.G., 1971. Particle motions in non-Newtonian media: I. Couette flow. Rheol. Acta 10, 344–364.

Gay, N.C., 1966. Orientation of mineral lineation along the flow direction in rocks: a discussion. Tectonophysics 3, 559–562.

Leal, L.G., 1975. The slow motion of slender rod-like particles in a second-order fluid. J. Fluid Mech. 69, 161–179.

Leal, L.G., 1992. Laminar Flow and Convective Transport Processes. Butterworth–Heinemann, Boston.

Leal, L.G., Hinch, E.J., 1971. The effect of weak Brownian rotations on particles in shear flow. J. Fluid Mech. 46, 685–703.

Manley, C.R., Fink, J.H., 1987. Internal textures on rhyolite flows as revealed by research drilling. Geology 15, 549–552.

Marsh, B.D., 1988. Crystal size distributions (CSD) in rocks and the kinetics and dynamics of crystallization: I. Theory. Contrib. Miner. Petrol. 99, 277–291.

Nichols, R.L., 1941. The velocity of the Big Obsidian Flow, Bend, OR. Trans. Am. Geophys. Union, 504–505.

Rahnama, M., Koch, D.L., Shaqfeh, E.S.G., 1995. The effect of hydrodynamic interactions on the orientation distribution in a fiber suspension subject to simple shear flow. Phys. Fluids 7, 487–506.

Shelley, D., 1985. Determining paleo-flow directions from groundmass fabrics in the Lyttelton radial dykes, New Zealand. J. Volcanol. Geotherm. Res. 25, 69–79.

Smith, J.V., Houston, H.C., 1994. Folds produced by gravity spreading of a banded rhyolite lava flow. J. Volcanol. Geotherm. Res. 63, 89–94.

Smith, J.V., Yamauchi, S., Miyake, Y., 1994. Coaxial progressive deformation textures in extrusive and shallow intrusive rocks, southwest Japan. J. Struct. Geol. 16, 315–322.

Stover, C.A., Koch, D.L., Cohen, C., 1992. Observations of fibre orientation in simple shear flow of semi-dilute suspensions. J. Fluid Mech. 238, 196–277.

Swanson, S.E., Naney, M.T., Westrich, H.R., Eichelberger, J.C., 1989. Crystallization history of Obsidian Dome, Inyo Domes, California. Bull. Volcanol. 51, 161–176.

Toramaru, A., 1989. Vesiculation process and bubble size distribution in ascending magmas with constant velocities. J. Geophys. Res. 94, 17523–17542.

Ventura, G., De Rosa, R., Colletta, E., Mazzuoli, R., 1996. Deformation patterns in a high-viscosity lava flow inferred from the crystal preferred orientation and imbrication structures: an example from Salina. Bull. Volcanol. 57, 555–562.

Wada, Y., 1992. Magma flow directions inferred from preferred orientations of phenocrysts in a composite feeder dike, Mikaye-Jima, Japan. J. Volcanol. Geotherm. Res. 49, 119–126.

Webb, S.L., Dingwell, D.B., 1990. Non-Newtonian rheology of igneous melts at high stresses and strain rates: experimental results for rhyolite, andesite, basalt and nephelinite. J. Geophys. Res. 95, 15695–15701.

Willis, D.G., 1977. A kinematic model of preferred orientation. Geol. Soc. Am. Bull. 88, 883–894.

Yarin, A.L., Gottleib, O., Raisman, I.V., 1997. Chaotic rotation of triaxial ellipsoids in simple shear flow. J. Fluid Mech. 340, 83–100.